
STRESS-STRAIN BEHAVIOUR OF COMPLETELY DECOMPOSED GRANITE IN BOTH TRIAXIAL AND PLANE STRAIN CONDITIONS

Md.Kumruzzaman^{1*} and Jian-Hua YIN²

^{1,2}*Department of Civil and Structural Engineering
The Hong Kong Polytechnic University
Hung Hom, Kowloon, Hong Kong, China*

*Corresponding Author: *kzzaman2001@hotmail.com*

Abstract: Most of the field problems in geotechnical engineering are in three dimensional states or close to a plane strain condition. Strength and deformation properties of soils in plane strain condition are considerably different from those in an axisymmetric condition. Many researchers have investigated the behaviour of soils under a plane strain condition. However, most of the previous studies have concentrated on sedimentary type of soils like sand and clay. Our understanding on the plane strain behaviour for residual soils is less than that for sedimentary soils. A true triaxial system with four sliding rigid-plates and real time feedback control has been used to test specimens of a completely decomposed granite (CDG) soil (a residual soil) under plane strain condition. The setup of the true-triaxial rigid plates is briefly introduced first. The preparation of soil specimens and testing procedures are described. The basic properties of the CDG are presented. The stress-strain and strength behaviour of the soil obtained under plane strain condition was investigated, and compared to the behaviour obtained under axisymmetric loading conditions. The results reveal that the critical state line in $q-p'$ space obtained under plane strain condition is the same as that under axisymmetric condition. However, the critical state line in $e - \ln p'$ space obtained under undrained plane strain condition is different from that under axisymmetric condition. The peak friction angle for plane strain tests is higher than that from axisymmetric loadings. It is also found that shear bands occur only in drained plane strain compression. Defuse bulging is the mode of failure for undrained plane strain as well as triaxial loading.

Keywords: *stress-strain, plane strain, axisymmetric, critical state line, friction angle, shear band.*

1. Introduction

The strength and deformation behaviour of geomaterials are often evaluated by using conventional triaxial compression tests, where a cylindrical soil specimen under axisymmetric loading condition is tested to simplify the field conditions. However,

most of the field problems, such as strip footings, embankments, and slopes are three dimensional or close to a plane strain condition. The stress-strain and strength behaviour under plane strain condition may differ from those measured under triaxial condition. To evaluate the soil behaviour in such cases, a variety of plane strain or true triaxial devices have been developed (Lade, 1978; Desrues *et al.*, 1985; Arthur *et al.*, 1985; Drescher *et al.*, 1990; Yasin *et al.*, 1999; Alshibli *et al.*, 2004; Wanatowski and Chu, 2006).

Comparative studies between plane strain and triaxial test results for granular soils have been performed by many researchers (Lee, 1970; Oda *et al.*, 1978; Marachi *et al.*, 1981; Alshibli *et al.*, 2003). The studies generally revealed that the plane strain specimens pose higher strengths than triaxial specimens. Increase of soil density and confining pressure has significant effect on the difference of strength parameters measured in triaxial and plane strain conditions. Failure strains of triaxial specimens are always larger than that of plane strain specimens. Another important difference between these test conditions for granular soils is the failure mode of specimens. The specimens in plane strain conditions fail with a well defined shear plane, whereas localized shear plane or bulging diffuse failure occurs in triaxial tests depending on the specimen density and confining pressure (Peters *et al.*, 1988). Alshibli *et al.*, 2003; Desrues and Viggiani, 2004 concluded that the stress conditions for plane strain and triaxial have a large effect on the strength of soil as well as shear band formation. Experimental findings for granular soils have shown that the failure of specimens subjected to plane strain loading condition is characterized by distinct shear bands (Han and Vardoulakis 1991; Finno *et al.* 1997; Chu *et al.* 1996; Alshibli *et al.* 2003), on the other hand, the triaxial specimens bulge uniformly and develop complex multiple shear bands at higher axial strain level (Alshibli *et al.* 2003). Complex shear banding in triaxial specimens of sand using the computed tomography has also been reported by Desrues *et al.* (1996) under a low confining pressure of 60 kPa..

Vaid and Campanella (1974) studied the behaviour of undisturbed marine clays under triaxial and plane strain loading conditions. The study concluded that specimens under plane strain condition show higher undrained strength and higher angle of shearing resistance than those under triaxial condition. Alshibli and Akbas (2007) also compared the behaviour of K_0 -consolidated kaolin specimens under those two conditions and the experimental results led to the same conclusion as that by Vaid and Campanella (1974). The test results also mentioned that the plane strain specimens fail with a well-defined shear band and triaxial specimens fail through a diffuse bulging mode. Peric and Hwang (2002) performed undrained plane strain testing on Georgia kaolin and pointed out the failure of the specimens with the shear bands as the specimens approach to the critical state regardless of stress histories and strain rates.

Several researches have been conducted to study the behaviour of soil in plane strain conditions. However, most of the previous studies have concentrated on sedimentary type of soils like sand and clay. Our understanding on the plane strain behaviour for residual soils is limited. Another important drawback in most of the previous studies on CDG soil is the absence of intermediate stress measurement. So the general stress-strain relationship for CDG soil was not achieved in most of the previous studies.

The objective of this paper is to study the behaviour of a residual soil (a completely decomposed granite soil) under plane strain and triaxial conditions. A true triaxial system with four sliding rigid plates that can be used to carry out plane strain tests is introduced first. The results of drained and undrained tests on the completely decomposed granite (CDG) are presented. The failure behaviour of the CDG measured under plane strain conditions is compared with that under triaxial conditions. The test results of CDG are also compared with the previous studies on sedimentary soils.

2. Test Equipment and Soil Samples

2.1 Triaxial Testing

A computer-controlled GDS triaxial testing system was used for performing saturation, consolidation and triaxial compression. Once the correct parameters were input, test could be automatically carried out by the GDS triaxial system with a computer feedback and control. The layout and schematic diagram of the GDS triaxial systems are shown in Figs. 1(a) and (b) respectively. The axial force was exerted on the test specimen by means of a piston fixed to the movable base pedestal. Axial displacements were measured by a GDS axial actuator which is a ball screw pushing the loading ram through the base of the cell. All the pressures were supplied and measured by means of deaired water. Back pressures were provided at the bottom of a specimen through the base pedestal, while pore water pressures were detected at the top of the specimen through the top cap. The hydraulic pressures (e.g. cell and back pressures) exerted on the triaxial specimen were supplied from the GDS pressure/volume digital controllers those are accurate to volume measurement of 1 mm^3 and pressure to 1 kPa.

2.2 True Triaxial System

Fig.2 (a) shows a true triaxial testing system with four rigid loading plates used for plane strain testing in this study. Details of the four sliding rigid plates design are presented in Yin *et al.* (2007). It shall be pointed out that the original loading plates provided by GCTS (2007) could not slide and a small gap between two plates should be left before testing. This original design had problems of (i) non-uniform stress/strain in the specimen and (ii) interferences of the plates at large strains (Yin *et al.* 2007). The

device includes four hydraulic load rams equipped with Linear Variation Displacement Transducers (LVDT). LVDT are placed outside the chamber along each piston for measuring displacement of the piston. The piston displacement is considered to be the displacement of the plate acting on the soil specimen and is used to calculate the compression or strain of the soil specimen. Each one of the horizontal loading rams has an internal load cell and there is only one load cell with the top vertical ram. Four sliding rigid plates (top and bottom; left and right) are used to apply two principal stresses.

A brick-shaped specimen of size 70 mm by 70 mm in horizontal plane and 140 mm in vertical height is enclosed in a rubber membrane of the same shape and size. The whole specimen is in membrane and the four sliding plates are all enclosed in a chamber as shown in the figure. Thus, the front and the back faces of the brick-shaped specimen are loaded by water pressure inside the chamber. The vertical and lateral stresses are applied using rigid plates and oil jacks and are respectively the major and intermediate principal stresses. The minor principal stress is applied by water pressure in the chamber. To reduce the effects of friction developing between the membrane and the sliding plates, 0.01mm thick plastic sheet with a thin layer of grease is used. GCTS (2007) pressure-volume controllers that have been used to measure pressure/volume are integrated with the true triaxial testing system. The system uses hydraulic digital servo control for maintaining the necessary test conditions.

Data during testing are logged electronically by a computer. All the transducers in the setup are connected to a controller through the computer interface unit for data acquisition and control. The controller itself is also connected to the computer. CATS software (developed by GCTS, 2007) automated various phases of testing such as consolidation and application of stresses. The universal test program is used by the universal as well as the triaxial and direct shear test modules of the GCTS CATS program. The universal test is the most flexible test in CATS. The universal test program is made up of numerous independent phases with each phase having independent duration, data acquisition and data saving selections, as well as analog, temperature and digital outputs control selections. There are numerous waveforms that can be executed on the outputs (analog or temperature), with the feedback for the outputs changeable between phases, as well as control the states of digital outputs. The setup of the true triaxial testing system is shown schematically in Fig. 2(b).

2.3 Basic Properties of the Completely Decomposed Granite Fill

The disturbed Completely Decomposed Granite (CDG) was taken from a slope site in Hong Kong. Specific gravity tests, particle size distribution tests, plasticity index tests, liquid index tests, standard compaction tests were done on the disturbed CDG soil. The percentage of soils finer than the No.200 sieve is about 52%. According to the Unified

Soil Classification System (USCS), the CDG soil is classified as sandy lean clay and the group symbol is CL. A summary of basic properties from these tests is presented in Table 1. The grain size distribution curve is shown in Fig.3a. Standard compaction test (Proctor test) shows the maximum dry density ρ_{dmax} of the CDG as 1.80Mg/m^3 with an optimum moisture content w_{opt} of 15.5% (Fig.3b). The dry density in most compacted fill slopes is 95% of the maximum dry density, that is, 1.71 Mg/m^3 .

2.4 Preparation of Samples and Testing Procedures

Laboratory reconstituted CDG was used in this study. A four part, square cross section split mould of inner dimension $70\text{mm} \times 70\text{mm} \times 140\text{mm}$ was used for the preparation of specimens. The CDG soil was compacted to 95% of the maximum dry density with 13% to 14% water content in five layers in the mould. The soil was compacted in five layers in the mould following the procedure described in ASTM standard D4767-95. At first, the oven dried soil mass was mixed thoroughly with water and then divided into five portions. Each portion of soil was then poured into the mould and was tamped gently to fill up the required volume. The top of each layer was scarified prior to the addition of material for the next layer. The tamper was used to compact the soil in layers inside the mould. After a specimen was formed, the specimen was then taken out from the mould and put into the membrane of the same size and shape. The thickness of the rubber membrane was 0.35mm. The open end of the membrane was sealed by a small piece of membrane using contact adhesive. Drainage facilities were provided at the top and bottom sides of the membrane to measure the volumes and pressures from both the top and bottom of the testing specimens. Split mould, membrane for specimen placement and specimen covered by membrane are shown in Fig.4 (a). Triaxial specimen (diameter 50.1mm and height 100mm) was also prepared in five layers with the same water content.

Placing the specimen into the true triaxial cell and connected the top and bottom outlet tubes to the pore pressure measurement transducers, the chamber was filled with deaired water. Turning the top water outlet opened, de-aired water was then used to flushing from the lower outlet tube and out of the upper outlet tube to remove entrapped air in the specimen maintaining the effective confining pressure 8 kPa in both cases. After one hour flashing and passing water through the upper outlet, a back pressure of 200 kPa was applied in all the tests. Skempton's B-value of 0.96-0.98 was obtained for all the specimens. After saturation, the specimen was consolidated isotropically under a confining pressure of 100 kPa, 200 kPa, and 400 kPa, respectively. Lateral sliding plates of the truly triaxial system was then moved to make a well contact between specimen and the rigid plates for plane strain testing. Keeping the lateral plates fixed in zero deformation control (i.e. $\epsilon_2 = 0$), vertical loading was then applied under a constant rate of deformation .

In triaxial testing, the compacted specimen was opened from the mould and placed on the bottom loading platen of GDS apparatus. Two porous stones (52 mm in diameter and 5.1 mm in thickness) were placed between the specimen and the loading platens in both top and bottom of the specimen together with filter paper of Whatman No. 41. Placing the top loading cap, the specimen was then covered by the membrane and both the ends of membrane were tighten with the loading caps using the o-rings. Placing the triaxial cell, saturation and consolidation were done similar to that of plane strain specimens. It is important to mention that Bishop and Green (1965) as well as Duncan and Dunlop (1968) carried out triaxial tests with lubricated and nonlubricated end platens. Schanz and Gussmann (1994) also carried out finite element simulations with or without lubricated end platen on triaxial specimens. All of them concluded that the sample geometry with or without end restraint does not have any significant influence on the shear strength measured during triaxial testing if the height to diameter ratio is greater than or equal to 2. Based on the above conclusions, the authors employed the conventional triaxial testing method without any lubricating end in all the triaxial testing with a height - diameter ratio about 2.0.

Triaxial and plane strain tests were conducted for both drained and undrained conditions. All experiments were performed in a deformation controlled mode at constant displacement rate of 0.01mm/min for drained tests and 0.03mm/min for undrained tests. Table 2 summarizes the tests conducted in this study and Fig.5 shows the loading control in both plane strain and triaxial testing.

3. Results of Plane Strain Compression Tests

3.1 Drained Condition

The stress-strain and volumetric behaviours of CDG under consolidated drained conditions of plane strain tests are shown in Fig.6. The deviator stress increases with the increase of confining pressure. Deviator stresses gradually increase with the increase of axial strain up to a strain level about 13~14%. Having some strain softening after this strain level, deviator stresses further increase to constant values at the end of the tests. Volumetric contraction is also observed until 13~14 % strain and with a little dilation the volumetric strains reach to constant values at the end. The changes of volume with respect to the increase of confining stresses are not pronounced. This is probably due to the stress states of plane strain condition or the particle size of CDG soils. Manifestation of shear bands was found to be formed in all three tests. The effective stress paths are shown in Fig.7 (a). The stress-ratio versus axial strain curves are shown in Fig. 7(b). It is clearly seen that the stress ratio varies within a narrow range of 1.39 and 1.41. Specimens at failure have reached at the state with continuous shear at global constant volume. The global volumetric response shows that the specimens have reached at

critical state. The slope of the critical state line in $q-p'$ space is 1.397. The coefficient of intermediate principal stress, $b = (\sigma_2 - \sigma_3) / (\sigma_1 - \sigma_3)$, at the critical state varies in the range of 0.17-0.18.

3.2 Undrained Condition

The results of undrained tests are presented in Fig.8 and Fig.9. It can be seen from Fig. 8 (a) that the deviator stress increases with the increase of confining pressures. A gradual increase of deviator stress without strain softening has been observed up to axial strain of 20%. The excess pore water pressure versus axial strain curves are shown in Fig.8 (b). It is shown that the excess pore pressures for lower confining stresses become constant after reaching the peak. But for higher confining pressure, there is a little decrease of pore water pressure after the peak and that is constant until the termination of the test. Excess pore pressures are always positive in all the tests. No shear band has been observed in undrained tests. The effective stress paths from these tests are plotted in Fig.9 (a). The CSL in $q-p'$ space from drained tests are also plotted in this figure. It is clear that the effective stress paths for undrained tests come close to the CSL of drained tests and move along that critical state line after the phase transformation where the specimens ended the contraction and started to dilate. As the pore water pressures are constant near the end of tests and the stress ratios are almost constant for all undrained tests, so critical state in $q-p'$ space is also achieved in undrained plain strain tests. The CSL in $q-p'$ space for both undrained and drained tests are measured as the same. The effective stress ratio versus axial strain curves are shown in Fig.9 (b). Same as drained tests, the b -value at failure varies within a range of 0.18~0.22.

4. Results of Triaxial Compression Tests

4.1 Drained Condition

The results of drained triaxial compression are shown in Fig. 10 and Fig.11. The stress-strain and volumetric behaviour are shown in Fig.10. Deviator stress and volumetric strain increase steadily with the increase of axial strain. Deviator stresses and volumetric strains are also increased with the increase of confining pressures and reached a constant value at the end of the tests. Positive volumetric strain (volumetric contraction) has been observed in all drained triaxial tests. The effective stress paths are shown in Fig.11 (a). The slope of critical state line in $q-p'$ plane is $M_{TCD} = 1.396$. Fig.11 (b) shows the curves for effective stress ratio versus axial strain and the stress ratio is almost constant, that is, 1.396 at the end of the tests. All the specimens in drained triaxial tests show bulging during shear up to axial strain of 20%.

4.2 Undrained Condition

The results of undrained triaxial compression tests on the same CDG are shown in Fig.12 and Fig.13. It can be seen from Fig.12 that both deviatoric stresses and pore water pressures increase with the increase of confining pressure. Test *CU03* (higher confined pressure) shows the strain hardening behaviour, but deviator stress finally reaches a constant value near end of the test. On the other hand, tests *CU01* and *CU02* (lower confined pressure) show the strain softening behaviour. The deviatoric stresses in these two tests reach the peak at lower axial strain and then reduce from the maximum value. The deviatoric stresses become constant as the strain further increases to the end of the tests. Positive excess pore water pressures have been observed for all specimens. Excess pore water pressure increases steadily with the axial strain and finally reaches a constant value at the end of the tests. As a result the critical state is also obtained in undrained tests. The stress paths in undrained tests are shown in Fig.13 (a). The CSL in $q - p'$ space from drained test has also been plotted on this figure. The $q/p' - \varepsilon_1$ plot for all undrained triaxial tests is shown in Fig.13 (b) and the stress ratio increases from zero to the M_{TCD} value monotonically. It is the same as drained tests that all specimens in undrained tests show the bulging failure at 20% axial strain.

5. Discussions of Triaxial and Plane Strain Compression Tests

5.1 Effective Stress Paths and Critical State Line in Compression

In triaxial compression tests, the vertical axial stress σ_a is the major principle stress σ_1 ; the horizontal radial stress σ_r is the minor and intermediate principle stresses, that is, $\sigma_3 = \sigma_2$. Therefore, the deviator stress, $q = \sigma_1 - \sigma_3$ and the mean stress is $p = (\sigma_a + 2\sigma_r)/3 = (\sigma_1 + 2\sigma_3)/3$. In terms of effective stress, $q = q'$, $p' = (\sigma'_a + 2\sigma'_r)/3 = (\sigma'_1 + 2\sigma'_3)/3$ and $p' = p - \Delta u_w$. In a compression test, the radial stress σ_r is kept constant ($d\sigma_r = 0$) and the axial stress is increased. The measured effective stress paths (ESP) are shown in Fig. 9(a) and other figures for other tests. The critical state line with a $M_{TCD} = 6 \sin \phi' / (3 - \sin \phi') = 1.396$ (friction angle $\phi' = 34.4^\circ$) is also shown in Fig. 9(a). It should be pointed out that the slope of $M_{TCD} = 1.396$ (or friction angle $\phi' = 34.4^\circ$) is the average value, which is determined from all 3 tests. All specimens were compacted in laboratory, which may not be exactly the same due to the hand compaction of the samples. Therefore, the final friction angle (or M_{TCD} -value) may vary slightly.

In a plane strain compression test after consolidation, the minor principal stress σ_3 is kept constant ($d\sigma_3 = 0$). After having made a good contact between horizontal loading plates and the specimen, the horizontal plates are kept no-displacement and the axial stress is then increased (loading), that is, $d\sigma_a \neq 0$. The vertical axial stress σ_a is the major principle stress σ_1 ; the horizontal stress σ_2 is the intermediate principal stress and σ_3 is the minor principle stresses. Therefore, the deviator stress, $q = \frac{1}{\sqrt{2}} [(\sigma_1 - \sigma_2)^2 + (\sigma_2 - \sigma_3)^2 + (\sigma_3 - \sigma_1)^2]^{1/2}$ and the mean stress is $p = (\sigma_1 + \sigma_2 + \sigma_3)/3$. In terms of effective stresses, $q = q'$ and $p' = p - \Delta u_w$. The measured effective stress paths (ESP) are shown in Fig. 5(a) and other figures for other tests. The critical state line in $q - p'$ space is found to have a slope of $M_{PSD} = 1.397$ (friction angle $\phi' = 42.1^\circ$) as shown in Fig. 5(a). According to the Mohr-Coulomb criterion, the friction angle is only dependent on σ_1' and σ_3' . So σ_1' and σ_3' values at critical state were used to calculate the ϕ' for the plane strain condition ($\phi' = \sin^{-1}[(\sigma_1' - \sigma_3') / (\sigma_1' + \sigma_3')]$).

A summary of the critical state lines for both plane strain and triaxial conditions in $q-p'$ space and $e-\log p'$ space are shown in Fig. 14 for all compression tests. The slope of $M_{TC} = 6 \sin \phi' / (3 - \sin \phi') = 1.396$ is averaged value with a friction angle $\phi' = 34.4^\circ$ for triaxial conditions. The slope of CSL line for plane strain condition (M_{PSC}) is also 1.397 and the corresponding friction angle is 42.1° .

5.2 Important Features Observed from Results of Compression Tests

A few distinguished features can be identified from the results of compression tests as follows:

- (a) The deviatoric stress in plane strain condition is always higher than that of triaxial condition. The deviatoric stress under a drained plane strain condition gradually increases up to 13~14% strain. With a little strain softening, the deviatoric stress increases again and finally reached a constant value at the end of the tests. Such a strain softening is due to the particle rearrangements before the formation of shear bands during the shear in drained plane strain tests. Whereas, deviatoric stress in drained triaxial tests gradually increases and being constant at the end of the tests. For undrained plane strain tests deviatoric stress gradually increases. Deviatoric stress in undrained triaxial tests is being constant after the peak. In all cases

deviatoric stresses of plain strain experiments are higher than that on the triaxial experiments.

- (b) Excess pore water pressure in undrained triaxial testing is little bit smaller than plane strain testing. Changes in pore pressure in plane strain are always larger than those under the corresponding triaxial conditions (Vaid and Campanella, 1974). Volumetric strain in drained triaxial test is always higher than the plane strain test. Alshibli et al. (2003) mentioned that volumetric strain of triaxial experiments is much higher than that of the plane strain experiments.
- (c) Large volumetric contraction has been observed in triaxial conditions as well as plane strain conditions. Like other granular materials, the authors were expected the volumetric dilation of CDG under dense conditions even at large strain. A higher percentage (about 52%) of fine content presents in the CDG tested here in this study. The presence of higher fine content probably suppresses the volumetric dilation and causes this contraction. Increase of fine content reduces the dilation as well as shear strength of CDG specimens (Kim *et al.*, 2006). The contractive behaviour of CDG is further observed in large and smaller direct shear box tests (Cheung *et al.*,1988). Such a contractive behaviour of CDG specimens in drained and undrained triaxial condition is also reported by Jeong *et al.* (2000) under the confining pressure of 98 kPa. Drained triaxial tests on CDG (called Masado in Japan) in dense state performed by Murata *et al.* (1988) further confirm the contractive behaviour of this soil under a high pressure up to 400 kPa. Murata *et al.* (1988) also mentioned that the saturated specimens pose lower strength than the specimens of natural water content.
- (d) The *CSL* obtained from tests on CDG are plotted in Fig.14 on both $q-p'$ and $e-\ln p'$ planes. It should be mentioned here that there are shear bands in drained plane strain tests. The global measurement of void ratios will be different from local void ratios in the shear bands at critical state and no measurement of local void ratios has been taken in this study. So the global void ratios for drained plane strain tests were not used in $e-\ln p'$ plane for comparison. All the test specimens in this experimental program were compacted to 95% of the maximum density. As mentioned earlier, the critical state line obtained from the drained and undrained plane strain testing is unique in $q-p'$ space. Such a unique *CSL* for both drained and undrained plane strain tests was observed for loose sand (Wanatowski and Chu, 2006). They also mentioned that under undrained condition, medium dense sand does not reach the failure line obtained from drained tests. The majority of existing data which address the uniqueness of a critical state line are based on the response of loose sands (Vaid *et al.* 1990; Been *et al.* 1991). For CDG, the slope of critical state line in $q-p'$ space is $M_{PSC}=1.397$ under plane strain and $M_{TC}=1.396$ under triaxial conditions. The corresponding friction angles at critical states are

$\varphi_{PSC} = 42.1^\circ$ and $\varphi_{TC} = 34.4^\circ$. Mooney *et al.* (1998) reported that the critical states of each test don't constitute a unique relationship in $e-p'$ plane in plain strain compression. However, Finno and Rechenmacher (2003) showed a unique relationship between void ratio and effective stress at critical state in drained plane strain tests. In the present study, compacted CDG with the same initial density shows a unique $e-\ln p'$ relationship at critical state in undrained plane strain tests. The critical state lines in $q-p'$ planes for triaxial and plane strain conditions are the same for CDG. So the critical state line in $q-p'$ plane is unique for all stress conditions. Unique critical state line in $q-p'$ plane for triaxial and plane strain conditions is also reported by Alshibli and Akbas (2007). On the other hand, however, critical state lines in $e-\ln p'$ plane for triaxial and plane strain conditions are not the same for the same CDG.

- (e) It was not the main objective of this paper to study the localization phenomenon in details. This study wants to show the failure mode of the CDG specimens under different stress conditions. After removing the tested specimens from the experimental setup failure mode of the specimens were observed. All the specimens in drained plane strain conditions have shown manifestation of conjugate shear bands (Fig.4 (b)) and the inclination of the shear bands varies between 45° and 55° . The inclination angles (θ) are expressed as the angle between minor principal stress direction and the plane of shear band. The inclination angles of shear bands according to Mohr-Coulomb criterion [$\theta = 45^\circ + \varphi'_f/2$] and Roscoe solution [$\theta = 45^\circ + \psi_f/2$] are around 66° and 45° , respectively. According to Arthur *et al.* (1977), the inclination angle of shear bands [$\theta = 45^\circ + (\varphi'_f + \psi_f)/4$] is around 56° . It can be concluded from the experimental results that the Mohr-Coulomb criterion overestimates the θ values. The present inclinations of the shear bands show that the Arthur solution is the upper bound and Roscoe solution is the lower bound. The conclusion made from this limited experiments is supported by the conclusions drawn from Alshibli and Strue (2000). In drained plane strain testing, very little strain softening occurred at about 13~ 14% strain. Fig.13 shows the lateral stress versus axial strain plotting for drained and undrained plane strain conditions. It can be seen in drained plane strain tests that there is drop of σ_2 at a strain about 13~14%. Such a little drop of σ_2 may not an indication of the onset of shear band formation. The large contraction may have created those shear bands in drained plane strain tests. On the other hand, no shear band has been observed in undrained plane strain testing. Few experimental studies (Han and Vardoulakis, 1991, Finno *et al.* 1997, Mokni and Desrues 1999) have been devoted strain localization in undrained tests on sand. Conjugate shear bands in drained plane strain tests has also been observed in sand (Alshibli *et al.* 2003, Oda *et al.* 1978, Desrues and Viggiani, 2004). Wanatowski and Chu (2006) observed the single shear band in plane strain compression on sand. Desrues and Viggiani (2004) reported that single band is not the only pattern of strain localization. They also

mentioned that depending on the boundary condition and the slenderness of the specimen, various patterns of shear bands may appear. In the present study, the failure mode off course in global for triaxial testing on CDG is marked as a diffuse bulging without shear banding as shown in Fig.4(c) for both drained and undrained conditions. Therefore, the experimental results on CDG revealed that drained plane strain loading is described by shear banding and undrained loading by diffuse bulging. Diffuse bulging is also the failure mode for axisymmetric loading on CDG.

6. Conclusions

This paper has presented experimental results of compression tests on completely decomposed granite (CDG) under triaxial and plane strain conditions and has examined the characteristics of the stress-strain behaviour of the soil. Based on the test results and their interpretation, the following conclusions may be drawn:

- (1) The plane strain specimens pose higher values of deviator stresses than triaxial specimens in both drained and undrained conditions. Except drained plane strain, the deviator stresses for all specimens gradually increase and finally become constant. Strain softening occurs in drained plane strain testing at a strain about 13~14%.
- (2) The excess pore water pressure is lower and volumetric strain is higher for triaxial loading than those for plane strain loading.
- (3) Stress ratio at critical state as well as the critical state line in $q-p'$ plane for plane strain loading is the same as that for triaxial loading. The corresponding friction angle for plane strain is about 22% higher than triaxial loading. The higher friction angle of plane strain testing in the present study supports the findings by Vaid and Campanella (1974), Marachi *et al.* (1981), Alshibli *et al.* (2003), Alshibli and Akbas (2007) and among others.
- (4) A unique $e-\ln p'$ relationship at critical state has been observed in undrained plane strain loading. The critical state lines in $q-p'$ planes for triaxial and plane strain conditions are the same. But, the critical state lines in $e-\ln p'$ plane are different for triaxial and plane strain conditions.
- (5) The failure mode of specimens subjected to plane strain loading under drained condition is shear-banding. On the contrary, uniform bulging is the mode of failure for plane strain loading under undrained condition as well as triaxial loading. So the mode of failure is different for different loading conditions.
- (6) The true triaxial equipment used to perform plane strain testing is suitable for the measurement of stress-strain under general 3D stress state by measuring the σ_2 value during shear.

Table1. Properties of the Completely Decomposed Granite (CDG) fill

Specific gravity (G_s)		2.65
The maximum dry density (ρ_{dmax})	Mg/m ³	1.80
The optimum moisture content (w_{opt})	%	15.5
Plastic limit (w_p)	%	22.7
Liquid limit (w_l)	%	32.8
Gravel content	%	1.0
Sand content	%	47.0
Fine content	%	52.0

Table 2. Summary of all experiments and main parameters

Test No.	Test Type	Consolidation state		Critical state				
		e_o	p' (kPa)	e_c	p' (kPa)	q (kPa)	ϕ' (deg.)	b
CD03	TC	0.420	401.3	0.345	748.3	1046.3	34.4	0.00
CD02		0.459	199.3	0.390	371.1	514.3		0.00
CD01		0.497	98.1	0.432	190.8	268.1		0.00
CU03		0.425	398.2	0.425	245.0	330.0	33.7	0.00
CU02		0.455	197.6	0.455	103.4	138.2		0.00
CU01		0.490	98.2	0.490	47.4	61.5		0.00
PSD03	PSC	0.439	402.3	0.374	959.2	1325.0	39.6	0.17
PSD02		0.473	200.7	0.410	489.1	692.0	40.5	0.17
PSD01		0.511	102.6	0.450	263.6	383.4	42.4	0.18
PSU03		0.448	404.6	0.448	298.8	433.1	42.4	0.18
PSU02		0.486	202.8	0.486	159.4	227.0	42.3	0.19
PSU01		0.512	102.35	0.512	71.8	106.2	45.0	0.22

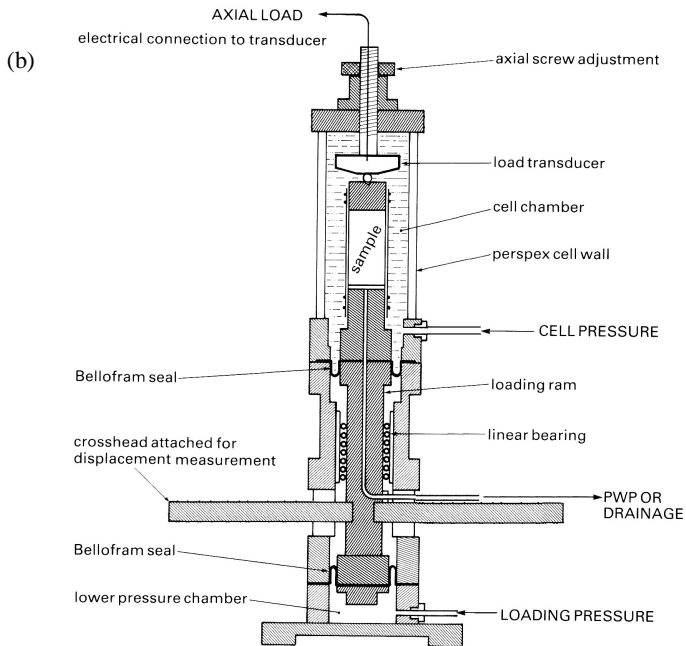
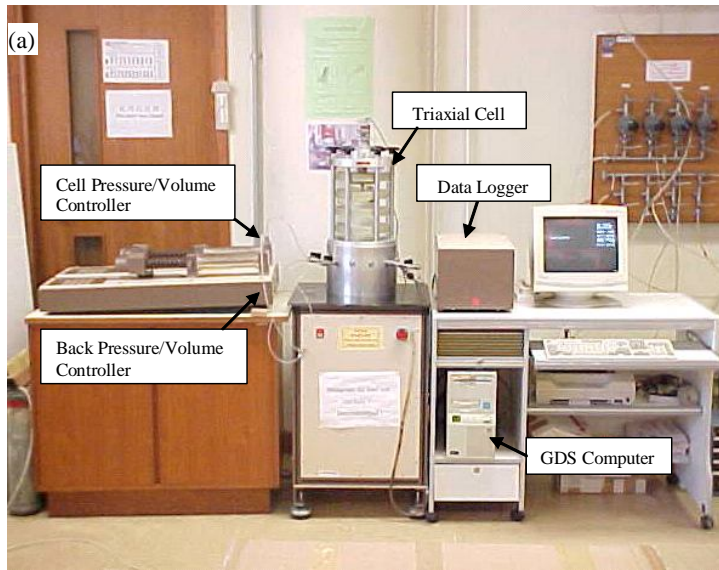


Fig.1. (a) A computer-controlled triaxial testing system for both static and cyclic loading (with 2Hz cyclic loading capability) and (b) a schematic diagram of the GDS triaxial cell (after Cheng and Yin 2005)

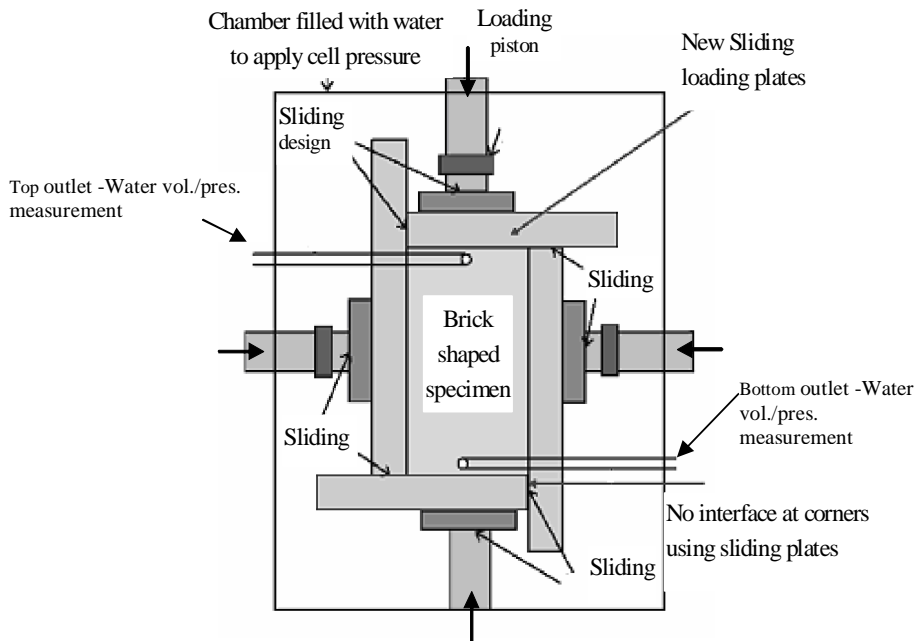
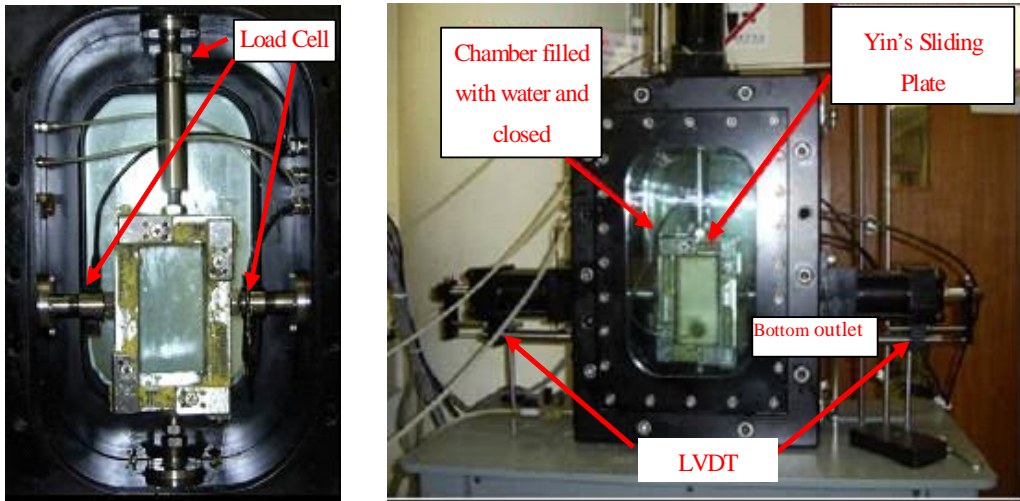


Fig.2. (a) A true triaxial cell with sliding plates (two photos and one diagram)

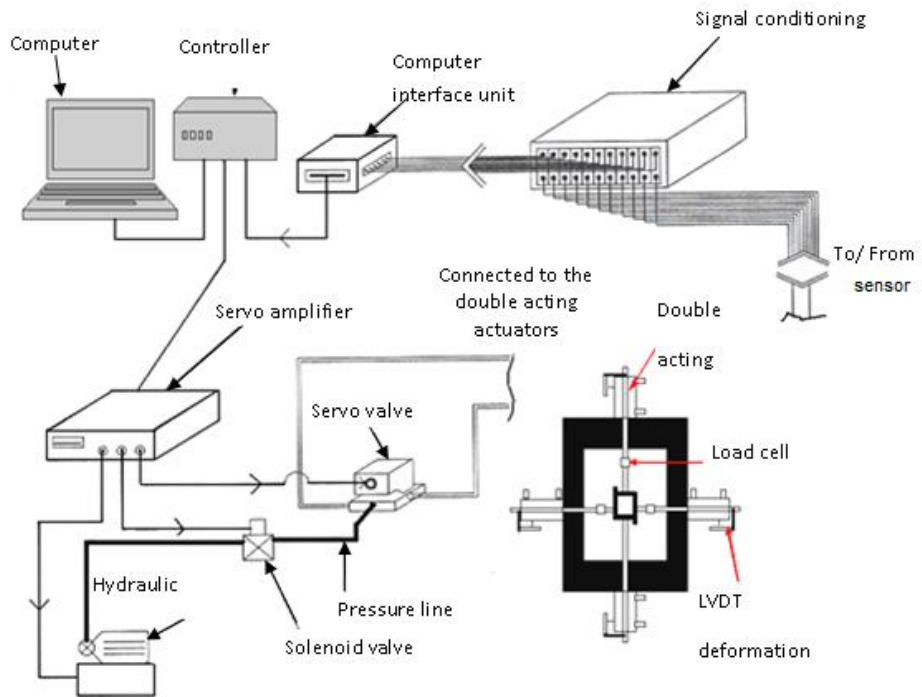


Fig.2. (b) setup of the true triaxial system

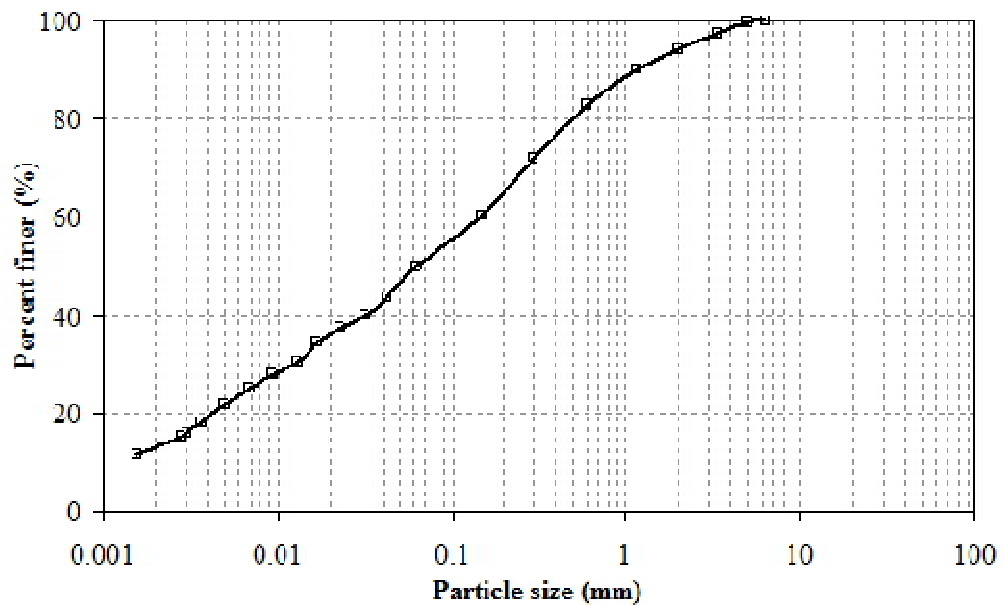


Fig.3. (a) Particle size distribution curve and

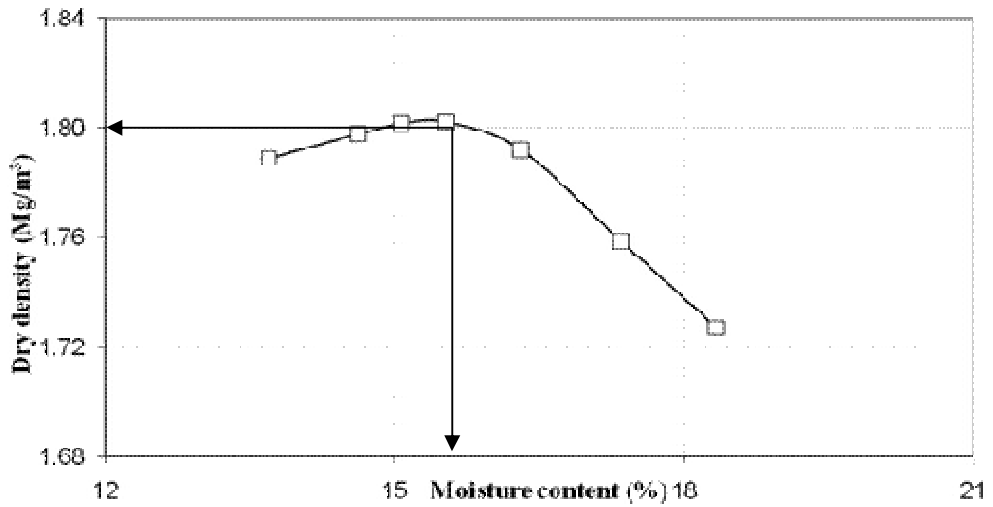


Fig.3. (b) Compaction curve for CDG

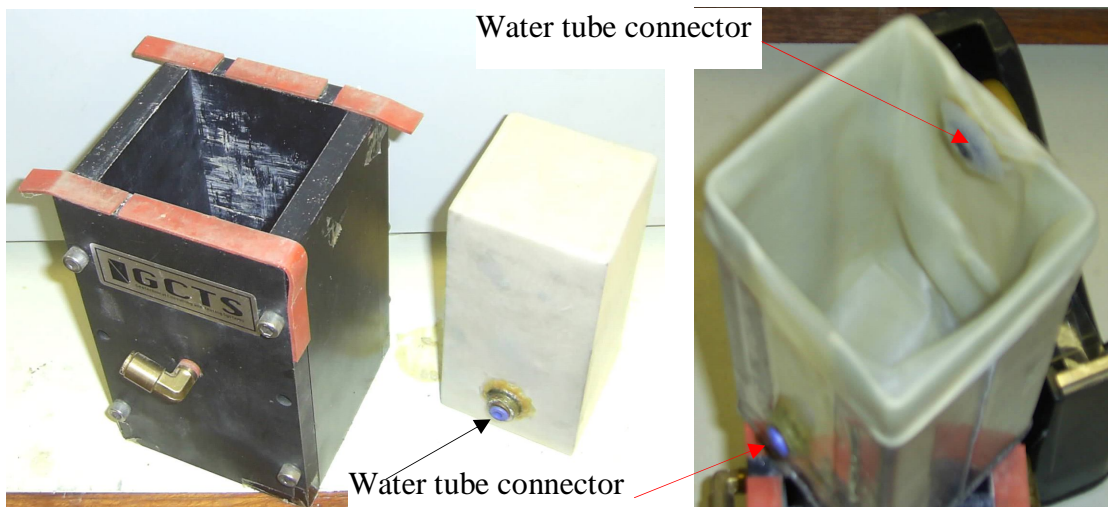


Fig.4. (a) A empty split mold (top left), a specimen fully enclosed by membrane with a water tube connector for water drainage or water pressure measurement (top middle), the mold overlaid with membrane (to right),

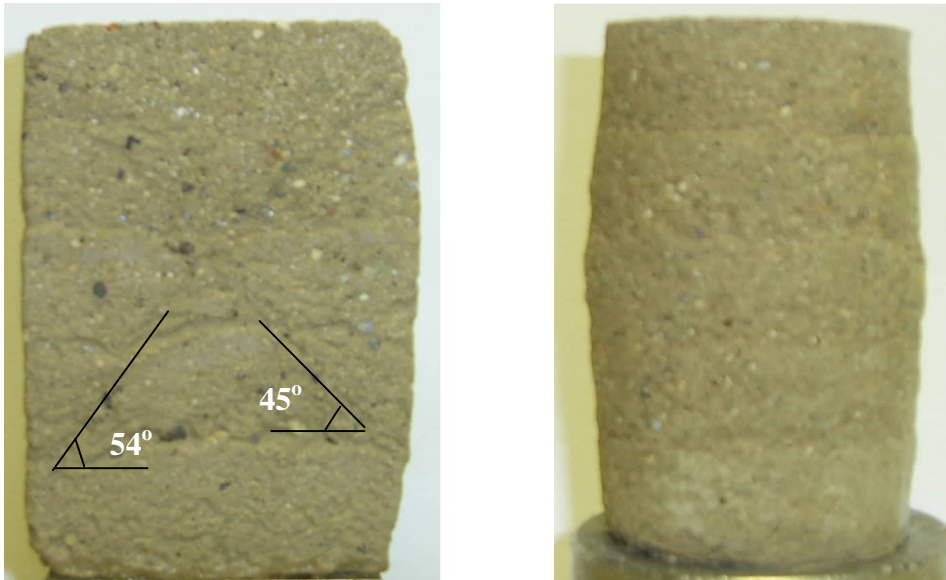


Fig.4. (b) a specimen after plane strain testing, and (c) a specimen after triaxial testing

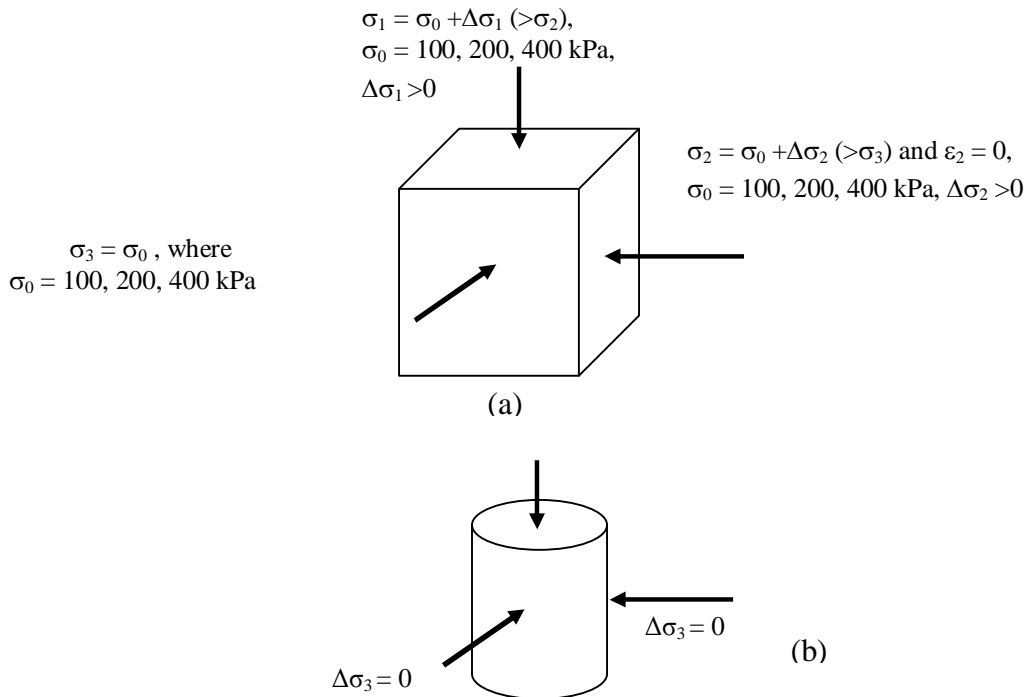


Fig.5 Control of loading in (a) plane strain and (b) triaxial conditions

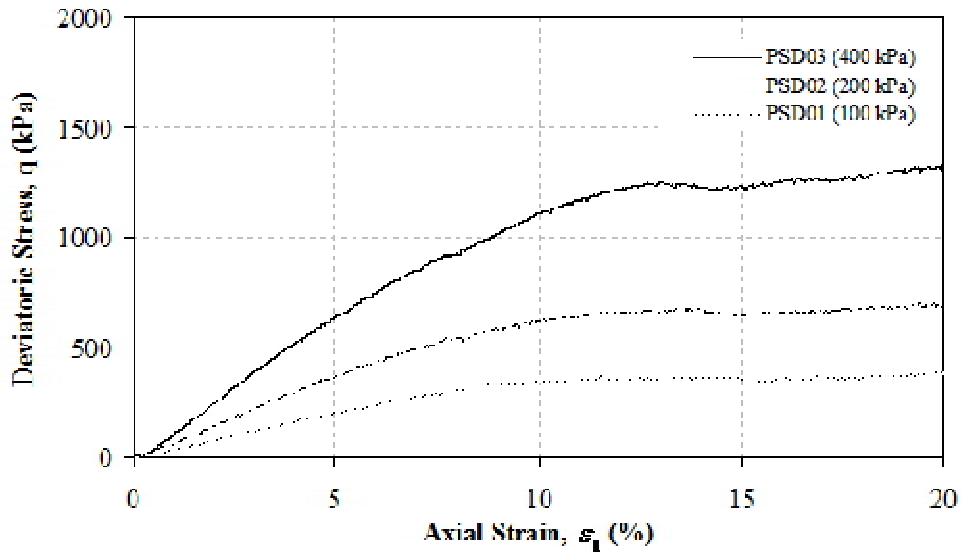


Fig.6. (a) Deviator stress versus axial strain

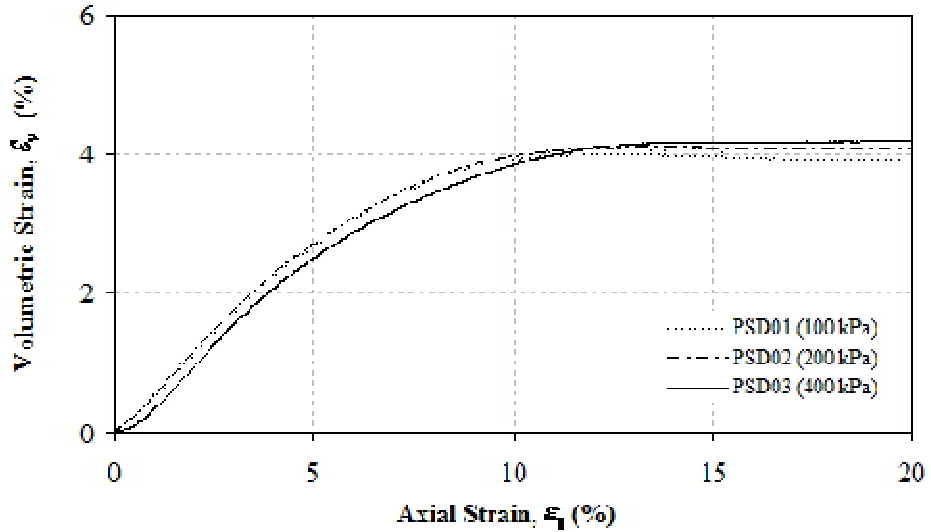


Fig.6. (b) volumetric strain versus axial strain under the confining stresses of 100, 200 and 400 kPa from consolidated drained plane strain tests

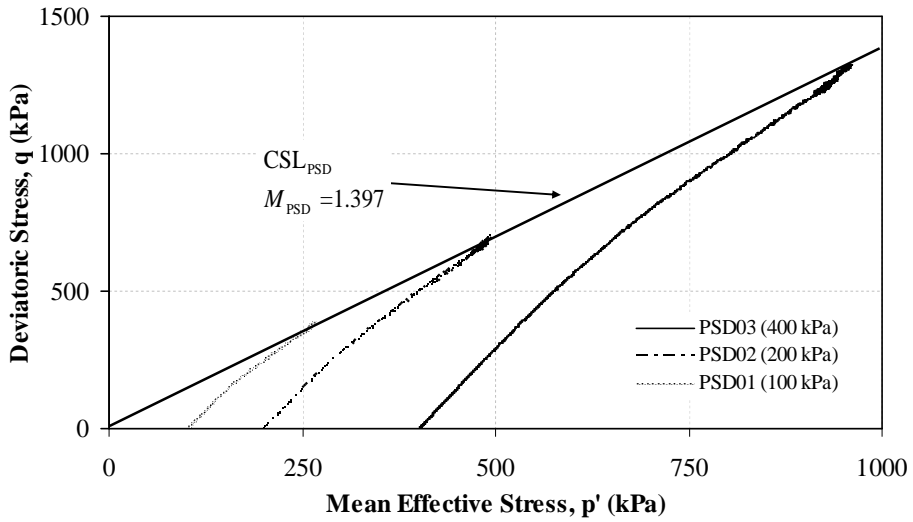


Fig.7. (a) Effective stress paths

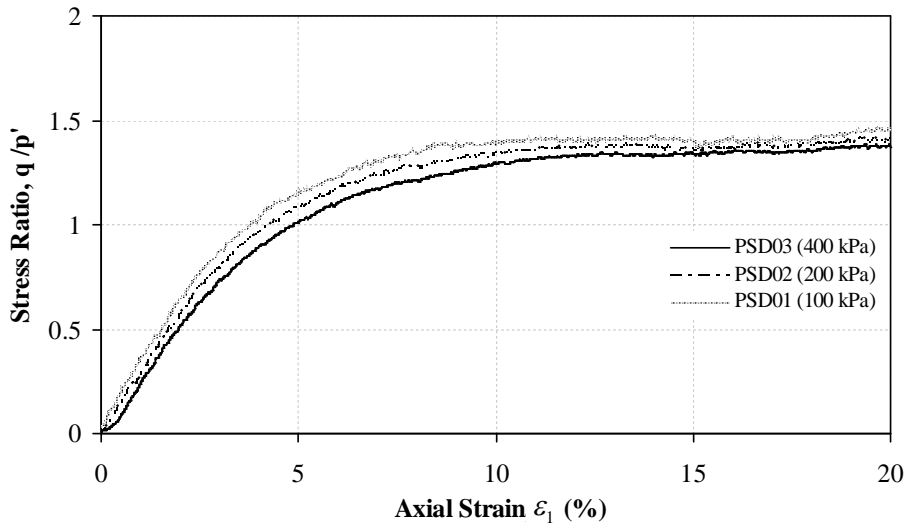


Fig.7. (b) stress-ratio versus axial strain under the confining stresses of 100, 200 and 400 kPa from consolidated drained plane strain tests

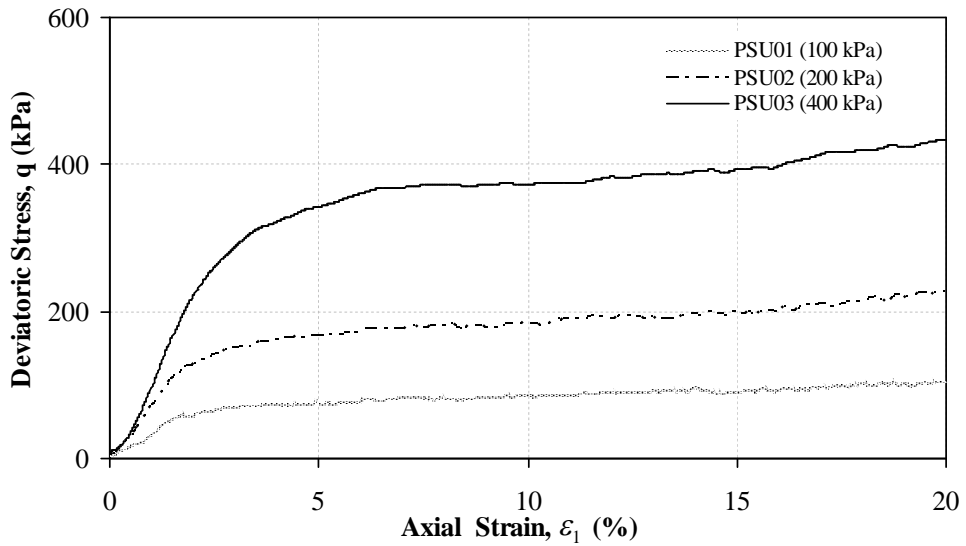


Fig.8. (a) Deviator stress versus axial strain

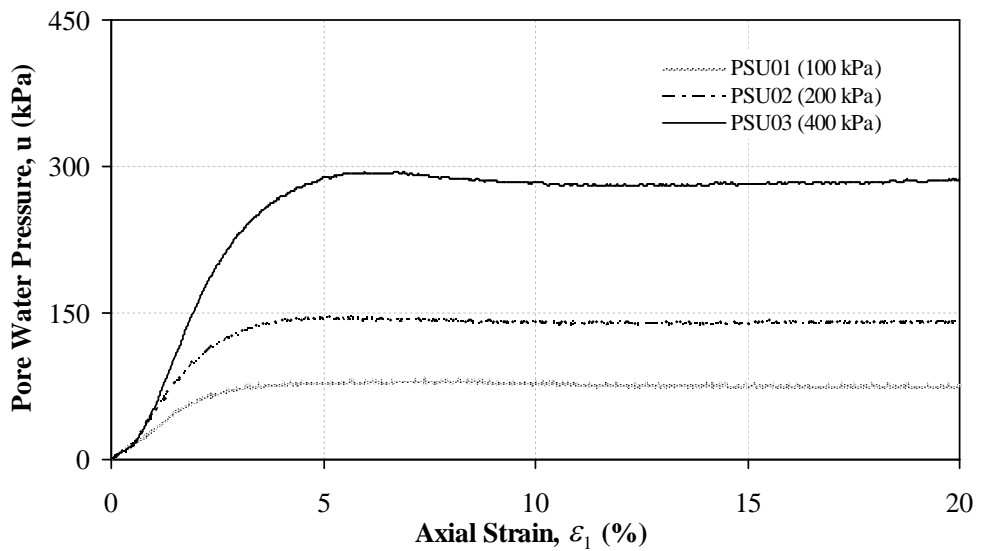


Fig.8. (b) pore water pressure versus axial strain under the confining stresses of 100, 200 and 400 kPa from consolidated undrained plane strain tests

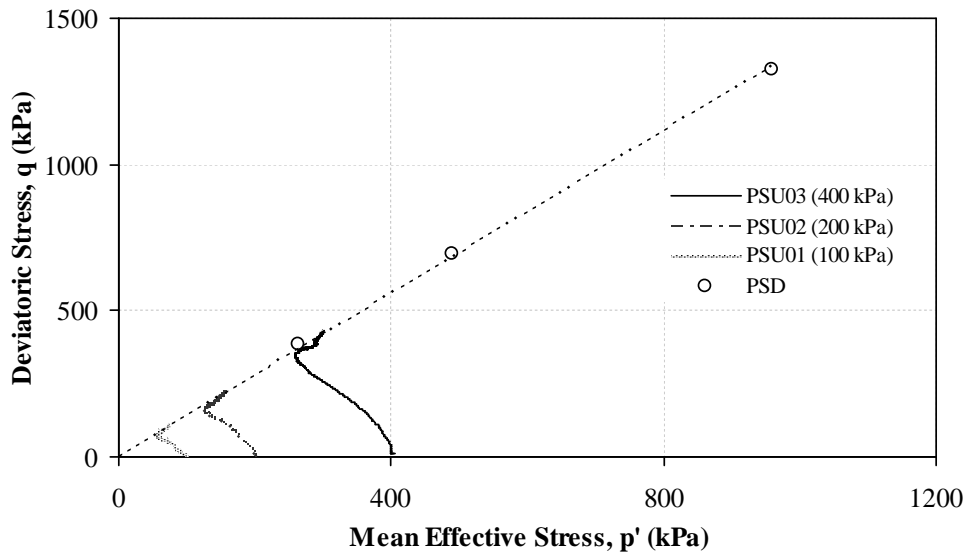


Fig.9. (a) Effective stress paths

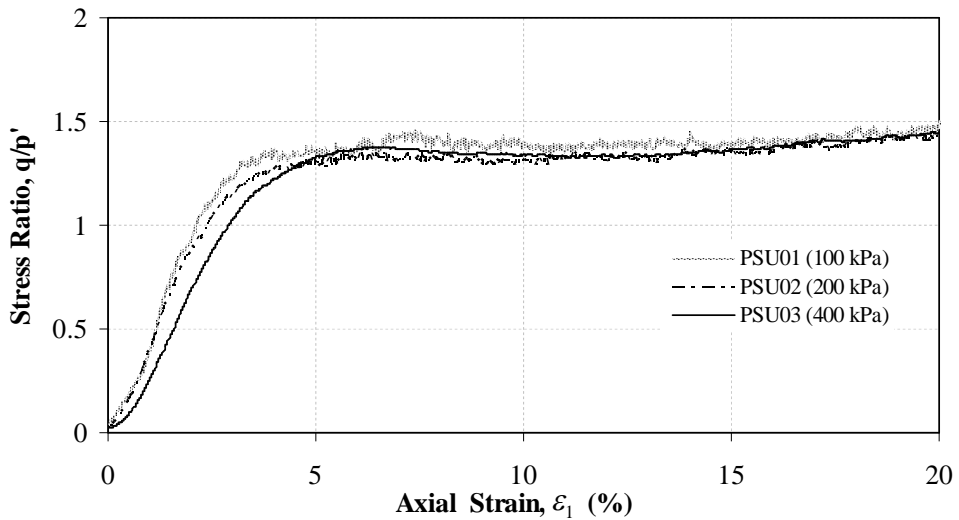


Fig.9. (b) stress-ratio versus axial strain under the confining stresses of 100, 200 and 400 kPa from consolidated undrained plane strain tests

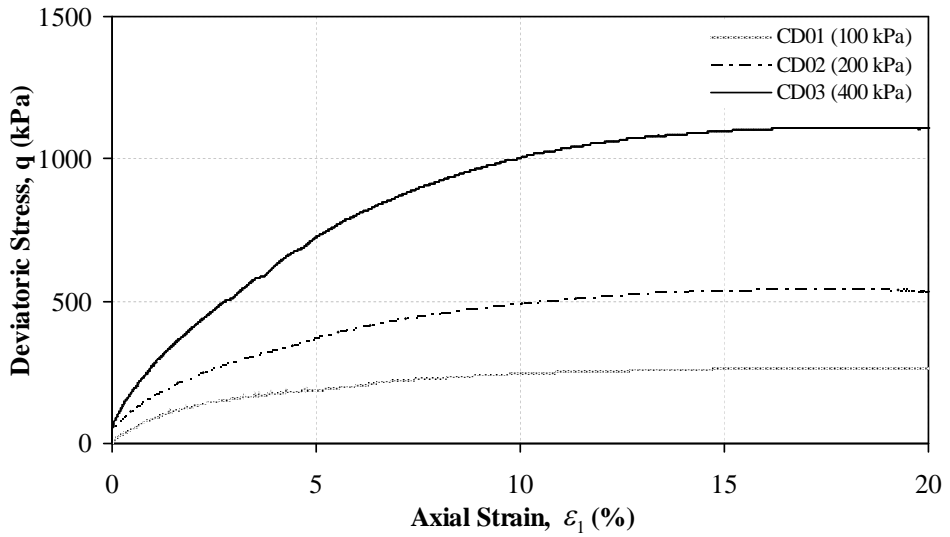


Fig.10. (a) Deviator stress versus axial strain

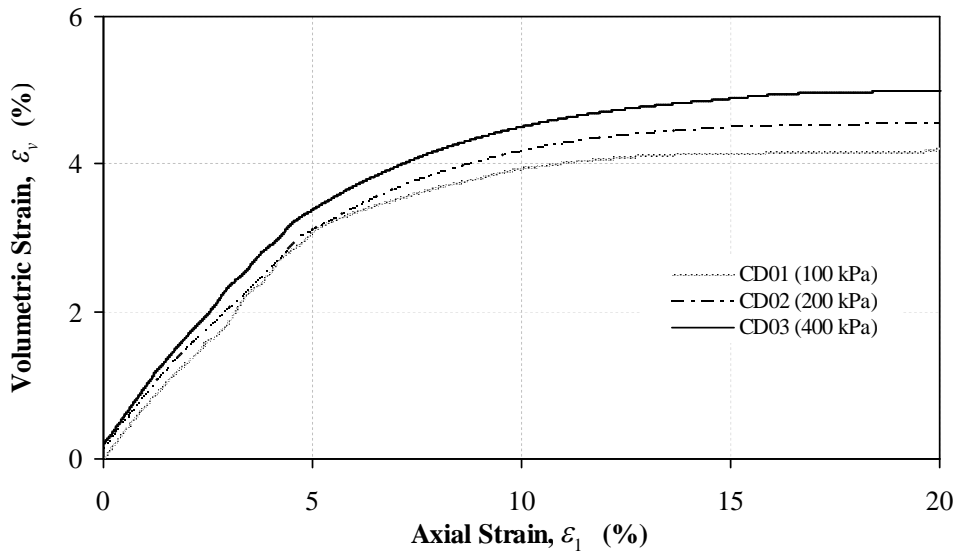


Fig.10. (b) volumetric strain versus axial strain under the confining stresses of 100, 200 and 400 kPa from consolidated drained triaxial tests

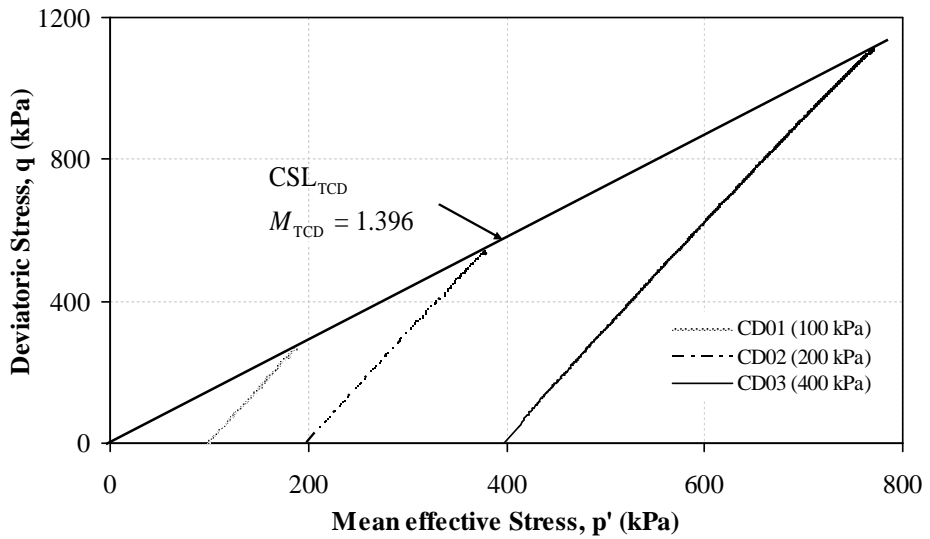


Fig.11. (a) Effective stress paths

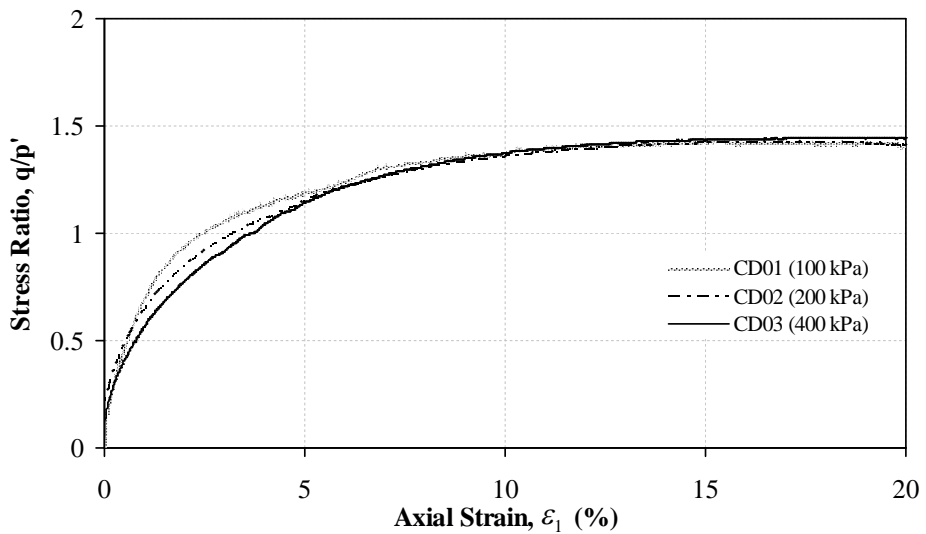


Fig.11. (b) stress-ratio versus axial strain under the confining stresses of 100, 200 and 400 kPa from consolidated drained triaxial tests

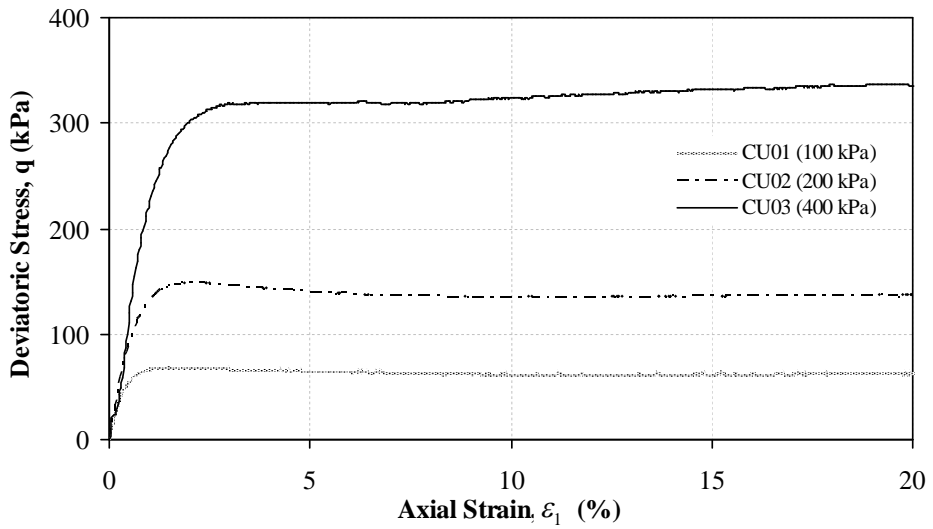


Fig.12. (a) Deviator stress versus axial strain

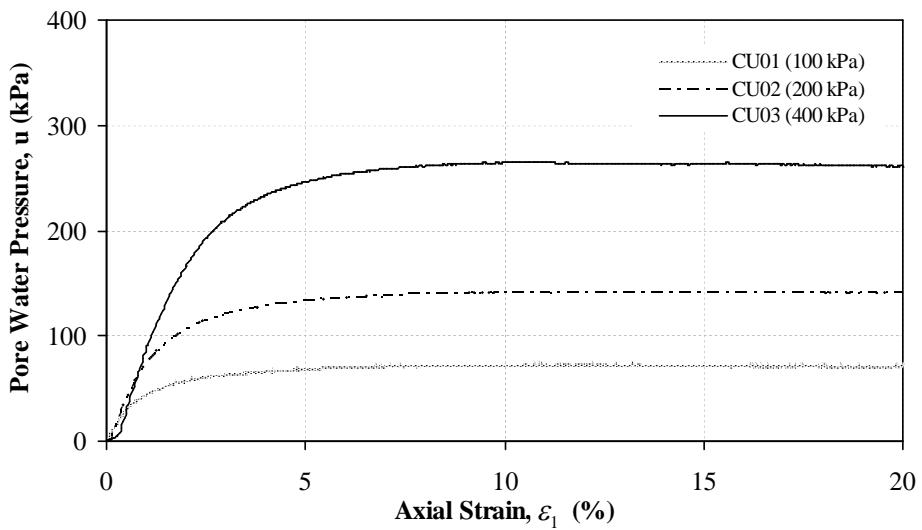


Fig.12. (b) pore water pressure versus axial strain under the confining stresses of 100, 200 and 400 kPa from consolidated undrained triaxial tests

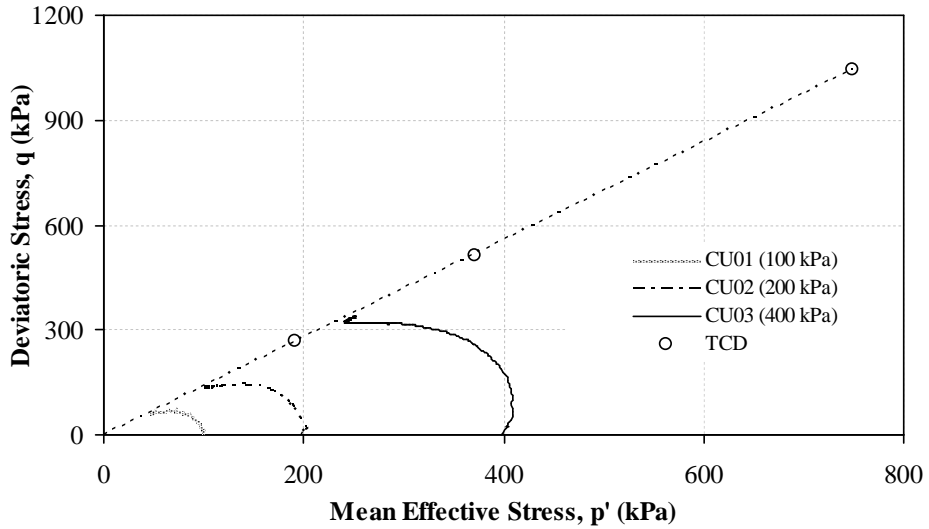


Fig.13. (a) Effective stress paths

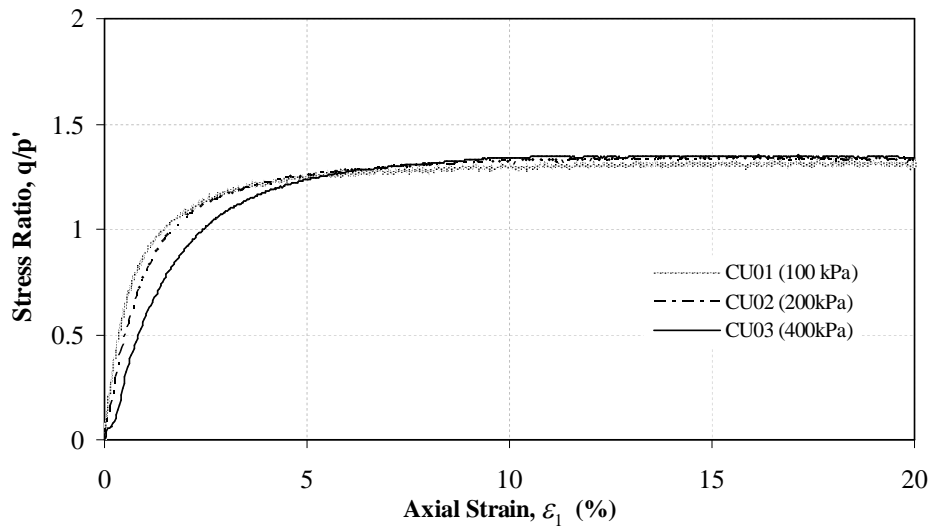


Fig.13. (b) stress-ratio versus axial strain under the confining stresses of 100, 200 and 400 kPa from consolidated undrained triaxial tests

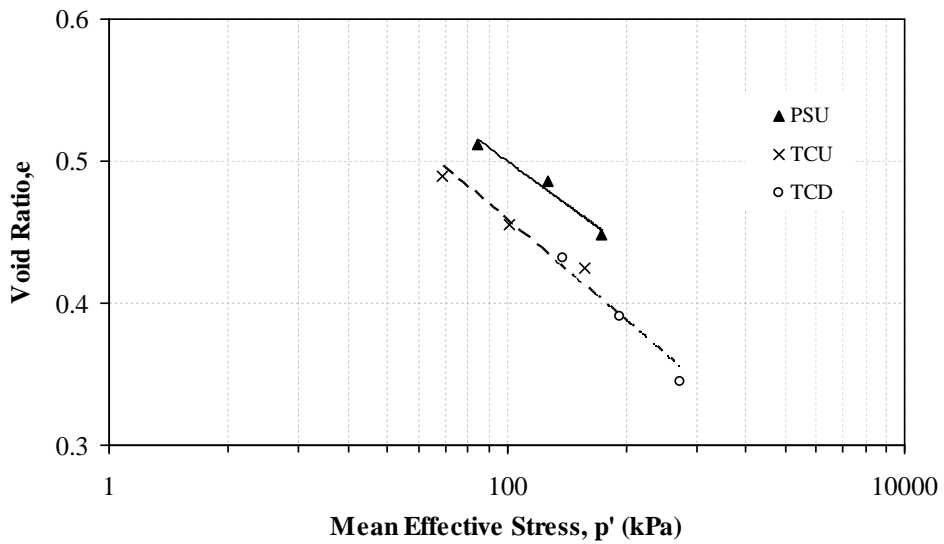
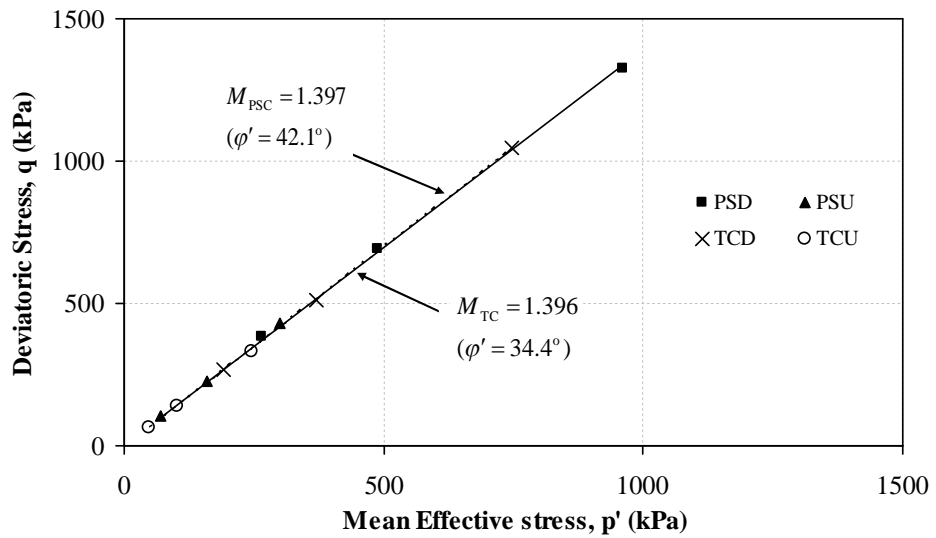


Fig.14. Critical state lines for plane strain and triaxial testing

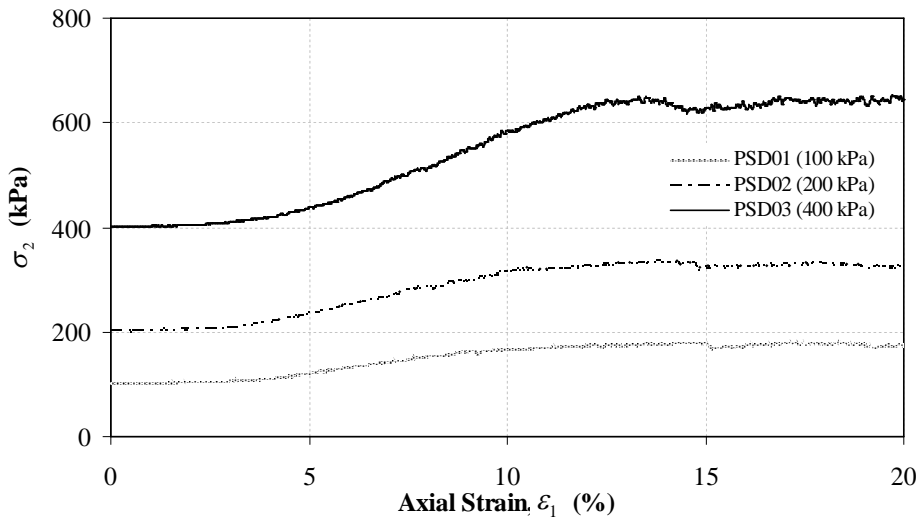


Fig.15. (a) Lateral stress versus axial strain for drained plane stress

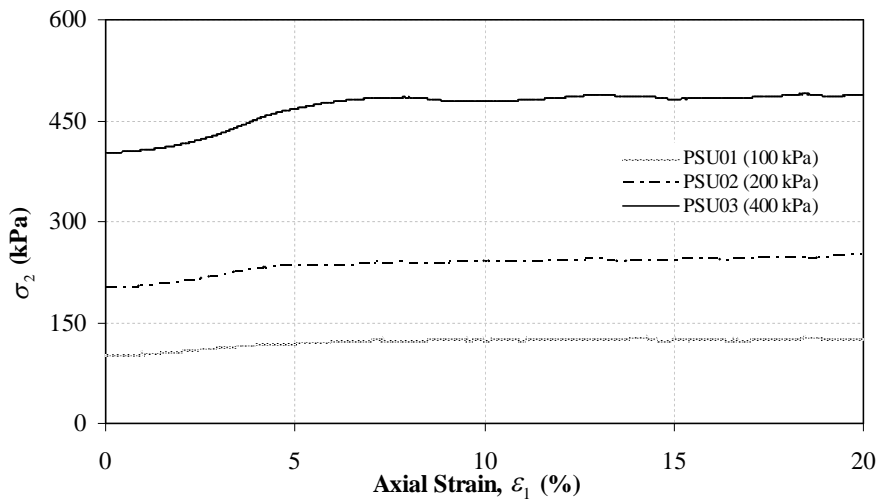


Fig.15. (b) Lateral stress versus axial strain for undrained plane strain tests

Acknowledgements

The work presented in this paper has received financial supports from a RGC grant of the University Grants Committee of the Hong Kong SAR Government of China and a grant from The Hong Kong Polytechnic University. These financial supports are gratefully acknowledged.

References

- Alshibli, KA. and Akbas, I.S. (2007) Strain localization in clay: plane strain versus triaxial conditions, *Journal of Geotechnical and Geological Engineering*, Vol.25, No.1, 45-55.
- Alshibli, KA. and Sture, S. (2000) Shear band formation in plane strain experiments of sand, *Journal of Geotechnical and Geoenvironmental Engineering, ASCE*, Vol.126, No.6, 495-503.
- Alshibli, KA., Batiste, S.N. and Sture, S. (2003) Strain localization in sand: plane strain versus triaxial compression, *Journal of Geotechnical and Geoenvironmental Engineering, ASCE*, Vol.129, No.6, 1-12.
- Alshibli, KA., Godbold, D.I. and Hoffman, K. (2004) The Louisiana plane strain apparatus for soil testing, *Geotechnical Testing Journal*, Vol.27, No.4, 1-10.
- Arthur, J., Dunstan, T., Al-Ani, Q. and Assadi, A. (1977) Plastic deformation and failure in granular media, *Geotechnique*, Vol.27, No.1, 53-74.
- Arthur, J.R.F., Dunstan, T. and Enstad, G.G. (1985) Determination of the flow function by means of a cubic plane strain tester, *International Journal of Bulk Storage in Silos*, Vol.1, No.2, 7-10.
- Been, K., Jefferies, M.G. and Hachey, J. (1991) The critical state of sands, *Geotechnique*, Vol.41, No.3, 365-381.
- Cheng, C-M. and J-H Yin (2005) Strain-rate dependent stress-strain behaviour of undisturbed hong kong marine deposits under oedometric and triaxial stress states, *Marine Georesources and Geotechnology*.
- Chu, J., Lo, S-CR. and Lee, IK. (1996) Strain softening and shear band formation of sand in multi-axial testing, *Geotechnique*, Vol.46, No.1, 29-42.
- Chung, C.K., Greenway, D.R. and Massey, J.B. (1988) Direct shear testing of a completely decomposed granite, *Proc. of 2nd Int. Conf. on Geomechanics in Tropical Soils. Publisher: A.A. Balkema, Singapore, 12-14 December*.
- Desrues, J. and Viggiani, G. (2004) Strain localisation in sand: an overview of the experimental results obtained in grenoble using stereophotogrammetry, *International Journal for Numerical and Analytical Methods in Geomechanics*, Vol.28, 279-321.
- Desrues, J., Chambon, R., Mokni, M. and Mazerolle, F. (1996) Void ratio evolution inside shear bands in triaxial sand specimens studied by computed tomography, *Géotechnique*, Vol.46, No.3, 529-546.
- Desrues, J., Lanier, J. and Stutz, P. (1985) Localization of the deformation in tests on sand sample, *Engineering Fracture Mechanics*, Vol.21, No.4, 909-921.
- Drescher, A., Vardoulakis, I. and Han, C. (1990) A biaxial apparatus for testing soils, *Geotechnical Testing Journal*, Vol.13, No.3, 226-234.
- Finno, R.J. and Rechenmacher, A.L. (2003) Effects of consolidation history on critical state of sand, *Journal of Geotechnical and Geoenvironmental Engineering, ASCE*, Vol.129, No.4, 350-360.
- Finno, R.J., Harris, W.W., Mooney, M.A. and Viggiani, G. (1997) Shear bands in plane strain compression of loose sand, *Geotechnique*, Vol.47, No.1, 149-165.

- GCTS (2007) True triaxial system and computer software manuals, *Developed by Geotechnical Consulting and Testing Services (GCTS), USA.*
- Han, C. and Vardoulakis, I. (1991) Plane-strain compression experiments on water-saturated fine-grained sand, *Geotechnique*, Vol.41, No.1, 49-78.
- Jeong, J., Kang, B., Lee, K. and Yang, J. (2000) Shear strength properties of decomposed granite soil in Korea, *Proc. of 8th Int. Conf. on Computing in Civil and Building Engg., Stanford University, August*, 14-16.
- Kim, D., Sagong, M. and Lee, Y. (2005) Effects of fine aggregate content on the mechanical properties of the compacted decomposed granite soils, *Construction and Building Materials*, Vol.19, 189-196.
- Lade, P.V. (1978) Cubical triaxial apparatus for soil testing, *Geotechnical Testing Journal*, Vol.1, No.2, 93-101.
- Lee, K.L. (1970) Comparison of plane strain and triaxial tests on sand, *Journal of Soil Mechanics and Foundation Division*, Vol.96, No.3, 901-923.
- Marachi, N.D., Duncan, J.M., Chan, C.K. and Seed, H.B. (1981) Plane-strain testing of sand, *Laboratory Shear Strength of Soil, ASTM STP 740, R. N. Yong and F.C Townsend, Eds.*, 294-302.
- Mokni, M. and Desrues, J. (1999) Strain localization measurements in undrained plane-strain biaxial tests on hostun rf sand, *Mechanics of Cohesive-Frictional Materials*, Vol.4, No.4, 419-441.
- Mooney, M.A., Finno, R.J. and Viggiani, M.G. (1998) A unique critical state for sand, *Journal of Geotechnical and Geoenvironmental Engineering, ASCE*, Vol.124, No.11, 1-12.
- Murata, H., Hyodo, M., and Yasufuku, N. (1988) Compression and shear characteristics of undisturbed residual soil 'Masado', *Proc. of Int. Conf. on Engineering Problems of Regional Soils. Beijing, China, August*, 11-15.
- Oda, M., Koshikawa, I. and Higuchi, T. (1978) Experimental study of anisotropic shear strength of sand by plane strain test, *Soils and Foundations*, Vol.18, No.1, 25-38.
- Peric, D. and Hwang, C. (2002) Experimental investigation of plane strain behaviour of georgia kaolin, *Numerical Models in Geomechanics-VIII, Pande GN and Pietruszczak S, Eds.*, 93-98.
- Peters, J.F., Lade, P.V. and Bro, A. (1988) Shear band formation in triaxial and plane strain tests, *Advanced Triaxial Testing of Soils and Rock, ASTM STP 977, R.T Donaghue, R.C. Chaney, and M.L. Silver, Eds.*, 604-627.
- Vaid, Y.P. and Campanella, R.G. (1974) Triaxial and plane strain behaviour of natural clay, *Journal of the Geotechnical Engineering Division*, Vol.100, No.GT3, 207-224.
- Vaid, Y.P., Chung, E.K.F. and Kuerbis, R.H. (1990) Stress path and steady state, *Canadian Geotechnical Journal*, Vol.27, No.1, 1-7.
- Wanatowski, D. and Chu, J. (2006) Stress-strain behaviour of a granular fill measured by a new plane-strain apparatus, *Geotechnical Testing Journal*, Vol.29, No.2, 149-157.
- Yasin, S.J.M., Umetsu, K., Tatsuoka, F., Arthur, J.R.F. and Dunstan, T. (1999) Plane strain strength and deformation of sands affected by batch variations and different apparatus types, *Geotechnical Testing Journal*, Vol.22, No.1, 80-100.
- Yin, J.H., Kumruzzaman, Md. and Zhou W.H. (2007) Laboratory facilities for measuring the stress-strain-strength behavior of soils- The State of the art, *Proceedings of the Fourth Cross-Strait Conference on Structural and Geotechnical Engineering, Zhejiang University Press*, 187-201.